Analysis on the Influence of Duct Casing Geometry on the Performance of a Ducted Fan

Marcellino V. Y. Pangaribuan[1*] & Firman Hartono[1]

[1]Faculty of Mechanical and Aerospace Engineering, Institut Teknologi Bandung, 40132, Bandung, West Java, Indonesia
*Email: marcellinopangaribuan@gmail.com

Abstract. This paper aims to evaluate the influence of an electric ducted fan's (EDF) geometry on its performance through parameter correlation analysis. Sample data was first built by generating new EDF models with varying duct casing geometries through optimal space-filling (OSF) sampling method. Afterwards, each model was simulated with computational fluid dynamics (CFD) to obtain each model's thrust, required power, and efficiency. It is found that the casing's inlet lip diameter displays the greatest influence on the EDF's total thrust, as the inlet diameter determines the casing's surface area affected by the low-pressure region ahead of the rotating fan blades. Additionally, it is found that length of the casing's exhaust lip affects the EDF's efficiency, while the exhaust lip diameter displays the highest correlation with the fan's required power.

Keywords: *computational fluid dynamics, electric ducted fan, optimal space-filling, parameter correlation analysis, performance.*

1 Introduction

According to Hu et al. [1], improvements and innovations on new technologies, such as new and efficient computational methods and sensors, have propelled the general market's interest on the development of unmanned aerial vehicles (UAVs) over the last two decades. Their remarkable agility, cost effectiveness, and flexibility to fulfill various purposes have made them popular for various purposes, such as for research, search-and-rescue, meteorological surveillance, or network extenders [2]. High demands have also initiated new research projects revolving around new concepts of propulsion systems for UAVs, ranging from propellers, jet engines, and even flapping wing designs. Among these propulsion systems, the one which presents the greatest potential is an electric ducted fan (EDF) [3].

A ducted fan is a propulsion system which consists of a rotor fan, a casing which envelopes around the rotor, and added extensions to the rotor's axis in the form of a nose cone ahead of the rotor and tail cone aft of it, thus forming the fan's hub [4, 5]. Sometimes, a set of stator blades or straighteners may also

Diterima 19 Januari 2024, Direvisi 23 April 2024, Diterima untuk dipublikasikan 6 Agustus 2024

ISSN:0852-6095, DOI: 10.5614/MESIN.2024.30.1.3

be added behind the fan blades. The added casing and hub will protect the fan blades from direct contact with external bodies/objects, thus reducing the risk of both blade damage and harm to the operators and/or bystanders [2, 5-7]. Moreover, an EDF unit is compact and flexible enough to be mounted at various positions on the craft, such as externally on a pod or embedded internally inside the craft's fuselage [6, 7]. The EDF's simplicity, due to the lack of complex fuel and ignition systems, such as spark plugs and pipes, makes the system cheaper and easier to produce [8].

However, the biggest benefit to the addition of these surfaces are the improvements to the fan's performance, as the fairings will allow the fan to generate greater thrust for equal of amount of power, thus improving the fan's efficiency, especially compared to the more conventional open rotor structure [9]. This is due to the EDF's casing which reduces generated tip loss by the fan blades, as well as generating more thrust [2, 9, 10].

The rise in popularity for ducted fans also raises the demand for various EDF designs suitable for specific requirements and environments. Unfortunately, research regarding in-depth analysis of an EDF's casing and hub is few and far between. The first significant research was developed by Schaller [9], where a 2D optimization of an EDF's casing was initiated, hence exhibiting a thrust increase by the fan and the casing by 3.1% and 24.5%, respectively. Furthermore, it was discovered that a reduction in the tip gap size by 2.5% of the fan's diameter would raise the system's thrust by 1.8% [9].

Experiments on duct casing designs were also conducted by Koç et al. [11], where 3 NACA casing airfoil profiles were investigated in comparison to an open propeller design. It was found that the casing raises the EDF's total thrust compared to that of an open propeller, thus improving its efficiency [11]. Further analysis was also initiated by Bontempo and Manna [12], where the influence of the casing's geometry on an EDF's performance was assessed by modifying the casing profile's section camber and the casing's cross section thickness based on NACA airfoil profiles. The paper concluded that thicker casing cross section and more significant camber profiles would result in greater duct thrust and propulsive efficiency [12]. However, as previous studies usually limit the casing's design on conventional airfoil profiles, it can be concluded that there is a need for deeper insight into how an EDF's performance is influenced by its geometry.

There are plenty of papers investigating various estimation methods to predict the performance of an EDF, with the most used method being computational fluid dynamics (CFD) [13]. While there are other methods which are capable of providing insight on an EDF's characteristics, such as through simple numerical

analysis codes [14, 15], CFD ensures that the generated numerical results will capture the complex airflow properties in the EDF, such as the generation of turbulent flows around the fan blades' trailing edges and the aft section of the EDF's casing and tail cone.

The main purpose of this study is to investigate how an EDF's casing geometry influences its performance, namely its thrust, required power, and fan efficiency. Analysis is initiated by generating a data sample of various casing geometries, along with their performance results which are obtained through CFD simulations. The obtained performance results will be evaluated to identify any substantial correlation between their thrust, required power, and efficiency, and their geometric parameters.

This research is aimed to provide further insight into optimization methods to modify an EDF's geometry to augment its resulting performance. For simplicity, this paper limits its investigation to the casing geometry of a conventional ducted fan, consisting of a row of fan blades, a row of stator blades behind them, as well as a duct casing, a nose cone, and a tail cone.

2 Methodology

In this paper, data sample was generated by ANSYS DesignXplorer 2019R3, while CFD simulation of each EDF model was carried out through ANSYS CFX 2019R3 to obtain the resulting performance parameters. Then, the obtained performance results and geometric data from the generated data sample will be evaluated with correlation analysis through ANSYS DesignXplorer 2019R3, thus providing insight on how the geometries of an EDF's hub casing will affect its performance. For clarity, the research procedure can be visualized as a flowchart, as shown in Figure 1.

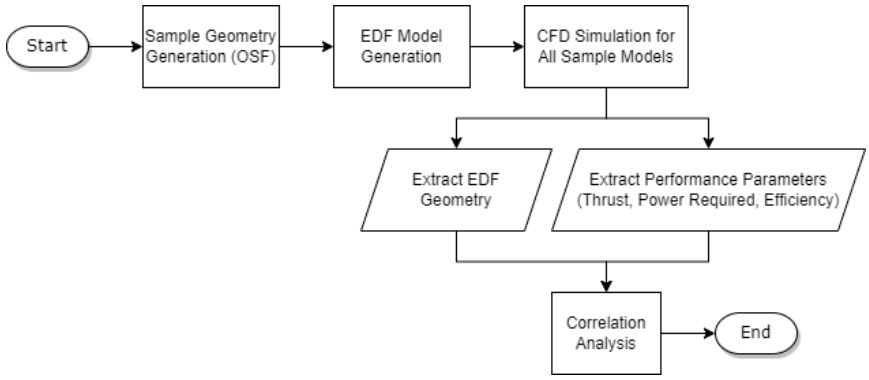

Figure 1 Flowchart for correlation analysis of the EDF

2.1 Ducted Fan Analysis

For this research, the ducted fan design that was chosen was a 195 mm EDF, which consists of 12 rotor blades, 7 stator blades aft of the rotors, a duct casing enveloping the rotor and stator blades, a nose cone and tail cone fairings as extensions to the fan's axial hub, as seen in Figure 2.

This EDF geometry, which would be dubbed the baseline EDF for the remainder of this paper, was a collaborative result between PT. CVD and ITB before further modification by Abdurrahman [16]. The basic performance of the baseline EDF is displayed in Table 1.

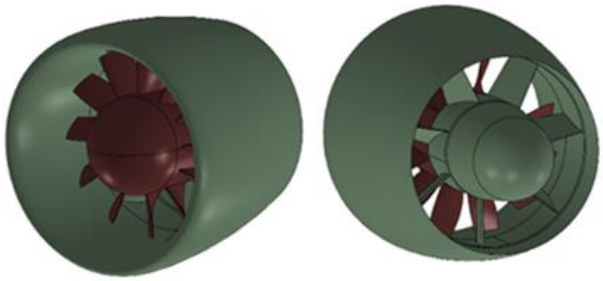

Figure 2 Visualization of the baseline 195 mm EDF

Table 1 Theoretical performance of the baseline EDF

Basic Dimension			Estimated Performance			
Dia	**Inlet area**	**Airpeed**	**Required power**	**Fan speed**	**Efficiency**	**Thrust**
195 mm	215 cm^2	100 m/s	15 kW	14000 RPM	80%	250 N

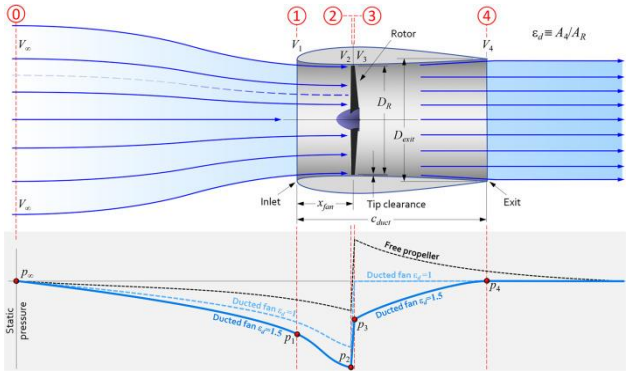

Figure 3 Idealized flow model of a ducted fan. The lower graph displays the change in static pressure along the stream tube's axial position [4]

The presence of a duct casing surrounding the fan will significantly improve the overall ducted fan's performance as the duct will also provide more thrust [2, 9, 10, 11]. Moreover, as shown in Figure 3, the duct's presence will reduce the power required to turn the fan as it effectively reduces the cross-section area of the rotor's stream tube, therefore accelerating the air flow, which not only reduces the required torque and power, but also generates a low-pressure region around the duct's inlet, thus raising the duct thrust [4, 17].

Within this paper, the EDF's predicted performance will be assessed by evaluating the EDF's total thrust and the fan's required power, as shown in Eq. (1) and Eq. (2), respectively.

$$T = \sum_{i=1}^{n} [p(i) + \tau_w(i)] \cdot dA_i \cdot \sin\theta_{xyz}(i) \tag{1}$$

$$P_{req} = \tau \cdot \Omega \tag{2}$$

Additionally, to assess the EDF's efficiency, the EDF's generated power will be obtained through Eq. (3). Finally, the EDF's propulsive efficiency can be defined as a ratio between the generated power and the fan's required power, as shown in Eq. (4).

$$P_{gen} = p_3 S_3 V_3 - p_2 S_2 V_2 \Longrightarrow P_{gen} = \Delta p_{23} S_f V_f \tag{3}$$

$$\eta = \frac{P_{gen}}{P_{req}} \tag{4}$$

2.2 CFD Simulation Setup

To assess the EDF's performance, CFD was utilized to predict the airflow characteristics around the rotating fan blades, as well as to obtain the system's total thrust and required power. However, to appropriately predict the effects of turbulence around the blades and the EDF's fairings, the most appropriate turbulence model must be chosen.

While there are a variety of turbulence models to choose from, few can efficiently fulfill a ducted fan's fluid flow simulation requirements. The simpler turbulence models, i.e. k-ε and k-ω, are only adequate for certain simulation cases, as the k-ε model is useful only for analyzing fluid flows within a freestream, while k-ω model is only useful in predicting fluid flows near the wall [18], whereas the more advanced models, i.e. RSM and LES, require unacceptable amount of computational power. According to Menter [18, 19], the most appropriate turbulence model, which is capable of modelling various

fluid flow cases with enough accuracy without the need for excessive computational power, is the SST k-ω turbulence model. Consequently, this turbulence model was selected to numerically simulate the EDF's performance.

To efficiently capture all relevant turbulent airflows, a grid independence test was initiated to select the appropriate mesh configuration. The result, as seen in Table 2, concludes that to obtain the most accurate EDF performance with the least amount of computational time and power, configuration number 4 were chosen to build the computational domain for the numerical simulation of the EDF. For clarity, Figure 4 is displayed to visualize the computational domain which was to be used for the EDF's numerical simulation.

Table 2 Result from the grid independence test

No.	Nodes	Elements	Thrust	Required Power	Efficiency
1	6,382,410	9,861,985	263.75 N	15.86 kW	73.95%
2	6,931,076	10,688,360	260.19 N	15.75 kW	71.36%
3	7,767,183	13,529,367	266.16 N	15.86 kW	74.38%
4	9,268,300	17,461,226	269.53 N	15.98 kW	75.92%
5	9,437,841	19,747,585	269.96 N	16.04 kW	76.57%
6	10,133,323	20,029,211	269.56 N	15.97 kW	75.80%
7	10,749,438	22,710,294	269.54 N	15.96 kW	75.90%
8	11,078,806	26,058,726	269.78 N	16.00 kW	76.38%
9	11,978,389	26,449,323	269.65 N	15.98 kW	75.78%

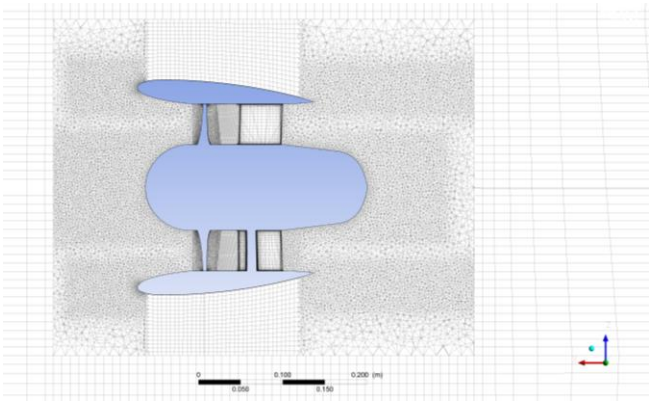

Figure 4 Cross section view of the mesh around the EDF

2.3 EDF Sample Generation

Sample generation is required to initiate a correlation analysis between the geometry of an EDF's casing and the resulting performance generated by the

EDF. As a result, the geometry of the EDF's fairings must be built from multiple, quantifiable parameters which are configurable by ANSYS DesignXplorer.

To achieve this, a single two-dimensional surface was first generated to act as a cross-section profile for all the EDF's fairings. This revolved surface was generated from 13 separate input parameters: input no. 1-8 to design the casing's leading edge, 9-11 for the casing's outer diameter, and 12-13 for the casing's trailing edge, each connected by b-spline functions for continuity. The input parameters for the revolved surface are displayed in Table 3 and Figure 5.

Table 3 Input geometry to build the EDF models, including the lower and upper limit of each parameter

No.	Nodes	Default [mm]	Lower Bound [mm]	Upper Bound [mm]
1	Inner casing radius 1	8.07	7.27	9.07
2	Inner casing radius 2	14.13	12.72	28.13
3	Inner casing radius 3	101.20	91.08	111.26
4	Inner inlet length	2.27	0.27	2.50
5	Inlet lip length	65.07	58.56	125.07
6	Inlet lip radius	119.65	99.56	135.65
7	Outer inlet length	10.51	3.51	18.51
8	Outer casing lip radius	6.40	3.76	9.04
9	Casing radius 1	127.82	115.04	140.60
10	Casing radius 2	123.89	111.63	136.28
11	Casing radius 3	113.53	107.21	125.53
12	Exhaust lip radius	102.00	91.86	135.00
13	Exhaust lip length	39.90	35.90	189.90

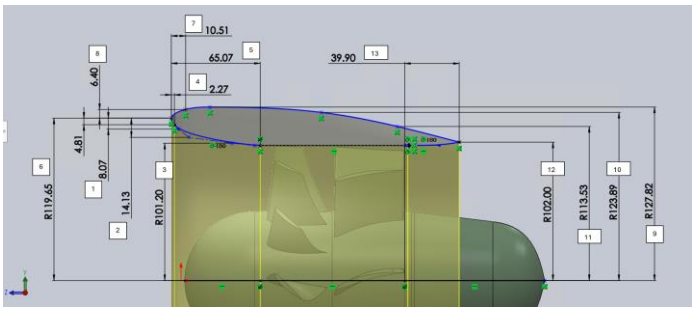

Figure 5 Revolved surface to generate the duct casing

With all the input parameters to generate new EDF models successfully defined, an adequate sampling method is required to generate an effective number of samples without excessive usage of computational power. One of the most

popular sampling methods is the Latin Hypercube Sampling (LHS). According to Queipo et al. [20], LHS is a random, stratified sampling method which distributes the input variables in a specific manner to ensure that each discrete input value is properly represented by a particular sample. However, ANSYS DesignXplorer also offers a refined form of the LHS, dubbed the Optimal Space-Filling (OSF) method [21]. While similar in concept, OSF adds a new iterative post process developed to maximize the distance between each data sample, hence resulting in a more evenly distributed data sample.

For this paper, 380 different samples, each with varying input parameters to generate different casing designs, have been generated. All ducted fan models will be analyzed through CFD simulations to obtain their performance parameters.

2.4 EDF Performance Correlation Analysis

The most appropriate analytical method must be chosen to assess the correlation between the casing geometry of the EDF's thrust, required power, and efficiency. For this paper, two correlation analysis methods were chosen: the Spearman correlation method [22], and the R^2 analytical methods [21].

2.4.1 Spearman Correlation Method

According to Pereira and Broed [22], Spearman correlation method is a correlation function which utilizes a ranking function to generate the Spearman coefficient (ρ) to define the association between the rank of input parameters and the rank of the resulting output parameters. Spearman correlation coefficient can be obtained through Eq. (5). Afterwards, a validation test must be conducted to assess the relevance of the obtained ρ through p-value calculation as seen in Eq. (6).

$$\rho = \frac{\Sigma_i (R_i - \bar{R})(S_i - \bar{S})}{\sqrt{\Sigma_i (R_i - \bar{R})^2}\sqrt{\Sigma_i (S_i - \bar{S})^2}} \Rightarrow \quad i = 1,2,\dots,N \tag{5}$$

$$\text{p} - \text{value} = 1 - A(t, df) \Rightarrow \; t = \frac{r_{XY}\sqrt{df}}{\sqrt{1 - r_{XY}{}^2}} \Rightarrow \; df = N - 2 \tag{6}$$

If the p-value is smaller than the significance level (α), which is α = 0.025 by default within ANSYS DesignXplorer [21], it can be concluded that there is a significant enough correlation between the input and output parameters which warrant further evaluation.

2.4.2 R^2 Correlation Method

R^2 correlation analysis would be initiated to identify any nonlinear (quadratic) correlation between the input parameters and the output parameters [21]. R^2 is defined as a ratio between the variance of a particular output parameter within a regressed response surface and the variance of the total output parameter, as shown in Eq. (7).

$$R^2 = 1 - \frac{\Sigma(y_i - \hat{y}_i)^2}{\Sigma(y_i - \bar{y})^2} \tag{7}$$

3 Results

3.1 Baseline EDF Simulation Result

The performance result of the numerical simulation for the baseline EDF model can be displayed in Table 4.

Table 4 Performance results for the baseline EDF

Thrust	Required Power	Generated Power	Efficiency
269.533 N	14000 RPM	12,130.30 W	75.925%

To provide additional visualization, the static pressure contour and velocity contour within the EDF can displayed in Figure 6 and Figure 7, respectively.

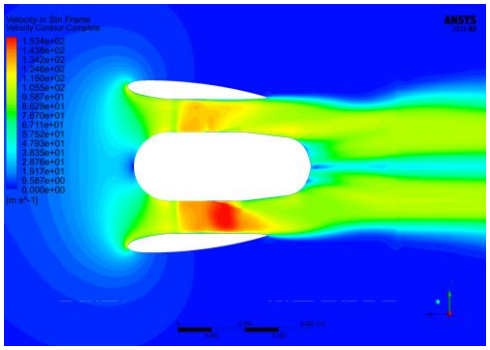

Figure 6 Velocity contour around the baseline EDF

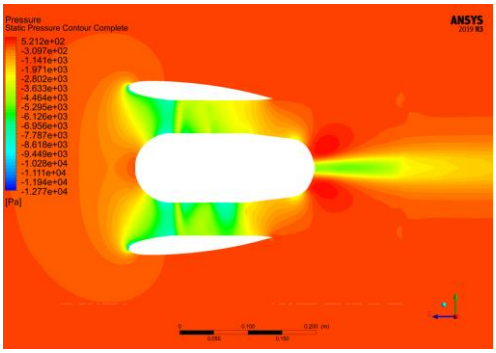

Figure 7 Static pressure contour around the baseline EDF

Figure 7 shows that there is a substantial low-pressure region just ahead of the rotating fan blades, thus implying that the inlet lip diameter contributes to the generated duct thrust. Additionally, there is a significant air flow separation on the trailing edge of the tail cone. Theoretically, this low-pressure pocket

indicates that there drag is generated at the rear end of the tail cone, thus reducing the EDF's efficiency and thrust.

3.2 EDF Correlation Analysis

As previously stated, 380 samples were numerically simulated through CFD to obtain their performance and analyze their correlation through Spearman correlation analysis and R^2.

3.2.1 Spearman Correlation Result

Through ANSYS DesignXplorer, a correlation matrix containing each input parameter's correlation with the ducted fan's performance can be generated. As the matrix is symmetrical, the ρ coefficient can be displayed in a simplified form, as shown in Table 5. For clarity, the blacked-out cells suggest that the relationships are not significant.

Table 5 Spearman correlation coefficient of each casing geometry input in relation to a conventional ducted fan's performance

No.	Input Param	Calc. ρ coeff.			p-value ($\alpha < 0.025$)		
		T	P. Req.	Eff.	T	P. Req.	Eff.
1	Inn. Cas. R. 1	0.044	-0.325	0.287	0.391	7.97E-11	1.27E-08
2	Inn. Cas. R. 2	0.092	-0.485	0.479	0.072	9.02E-24	3.44E-23
3	Inn. Cas. R. 3	0.077	0.678	-0.731	0.132	1.97E-52	8.63E-65
4	Inn. Inlet L	0.151	0.008	-0.047	0.0032	0.881	0.364
5	Inlet Lip L	-0.165	0.353	-0.440	0.0012	1.37E-12	2E-19
6	Inlet Lip R	0.388	-0.518	0.621	3.93E-15	1.61E-27	6.95E-42
7	Out. Inlet L	0.011	0.179	-0.126	0.829	0.0005	0.0143
8	Out. Cas. Lip R	0.179	-0.188	0.282	0.0005	0.0002	2.14E-08
9	Cas. R. 1	-0.156	-0.051	-0.010	0.0022	0.325	0.839
10	Cas. R. 2	-0.151	0.018	0.021	0.0032	0.727	0.684
11	Cas. R. 3	0.091	0.372	-0.295	0.075	6.42E-14	4.3E-09
12	Exh. Lip R	-0.344	0.353	-0.248	5.58E-12	1.42E-12	1.03E-06
13	Exh. Lip L	-0.356	-0.131	0.145	8.67E-13	0.0104	0.0046

It is found that the EDF's thrust displays the greatest amount of linear relation with the casing's inlet radius (ρ = 0.388), exhaust lip length (ρ = -0.356), and exhaust lip radius (ρ = -0.344). This suggests that there is a low to moderate positive relationship between the casing's inlet radius and the ducted fan's total thrust. Meanwhile, the duct casing's exhaust lip radius and lip length display a low moderate negative relationship with the thrust.

Table 5 also shows that there is a moderate to high positive relationship between the Inner Casing Radius 3 with the ducted fan's required power (ρ = 0.678), while a moderate negative relationship is found with the ducted fan's inlet radius (ρ = -0.518) and the Inner Casing Radius 2 (ρ = -0.485).

From an efficiency standpoint, the ρ coefficient from Table 5 suggest that there is a moderate to high negative relationship between Inner Casing Radius 3 and the EDF's efficiency (ρ = -0.731), while a moderate to high positive relationship is found between the inlet radius and the efficiency (ρ = 0.621).

3.2.2 R^2 Correlation Result

Through ANSYS DesignXplorer, the obtained quadratic R^2 determination of each input parameter in relation with the ducted fan's performance can be displayed, as seen in Table 6.

Table 6 R^2 quadratic determination of each casing geometry input in relation to a conventional ducted fan's performance

No.	Param	Quadratic Determination (R^2)		
		Thrust	P. Req.	Eff.
1	Inner Casing Radius 1	1.06%	16.97%	10.12%
2	Inner Casing Radius 2	2.35%	25.08%	18.85%
3	Inner Casing Radius 3	0.62%	50.39%	37.05%
4	Inner Inlet Length	3.53%	8.53%	5.22%
5	Inlet Lip Length	4.26%	17.19%	17.75%
6	Inlet Lip Radius	21.17%	32.13%	35.86%
7	Outer Inlet Length	0.12%	5.49%	1.79%
8	Outer Casing Lip Radius	5.87%	10.83%	10.97%
9	Casing Radius 1	2.67%	6.18%	5.94%
10	Casing Radius 2	1.70%	20.59%	9.55%
11	Casing Radius 3	0.19%	18.61%	6.52%
12	Exhaust Lip Radius	15.34%	26.11%	35.75%
13	Exhaust Lip Length	10.99%	7.00%	12.07%
	Full Model R^2	51.36%	75.87%	69.32%

The data from Table 6 suggests that 3 input parameters display significant R^2 values with the ducted fan's thrust, which are the inlet lip radius (21.17%), the exhaust lip radius (15.34%) and the exhaust lip length (10.99%), which is similar to the observations obtained from the Spearman correlation analysis. Additionally, the full model R^2 value of 51.36% suggests that the correlation

between the casing's geometry and the thrust can be moderately approximated as a quadratic correlation.

Table 6 also displays that there are 4 input parameters which display significant R^2 values with the ducted fan's required power: the Inner Casing Radius 3 (50.39%), inlet lip radius (32.13%), exhaust lip radius (26.11%), and Inner Casing Radius 2 (25.08%). It can also be seen that the full model R^2 of 75.87% signifies a moderate to good accuracy for quadratic correlation to approximate their correlation.

Lastly, the data from Table 6 shows that there are 3 input parameters which display significant R^2 values with the ducted fan's efficiency: the Inner Casing Radius 3 (37.05%), inlet lip radius (35.86%), and exhaust lip radius (35.75%). Moreover, with a full model R^2 of 69.32%, it can be deduced that quadratic correlation provides a moderate to good accuracy to approximate their relation.

3.2.3 Correlation Analysis

Table 7 is displayed to summarize the most significant input parameters which will affect an EDF's performance. Further analysis is focused on the input parameters shown below.

Table 7 Input geometries which display the best linear and quadratic correlation with the EDF's performance

Input Param	ρ	R2	Performance Variable
Inlet Lip Radius	0.388	21.17%	Thrust
	-0.518	32.13%	Power Required
	0.621	35.86%	Efficiency
Inner Casing Radius 3	0.678	50.39%	Power Required
	-0.731	37.05%	Efficiency

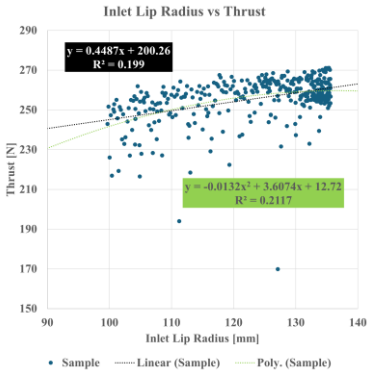

Figure 8 Scatter plot for thrust against inlet lip radius

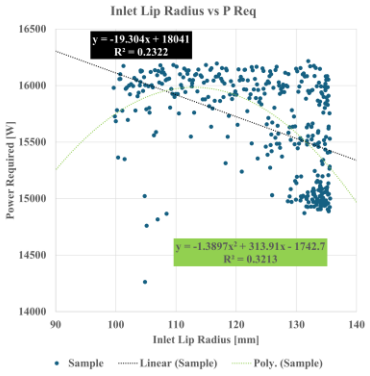

Figure 9 Scatter plot for power required against inlet lip radius

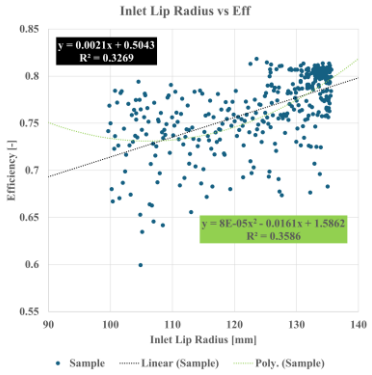

Figure 10 Scatter plot for efficiency against inlet lip radius

The widespread distribution of the obtained thrust values on all the scattered plots can be explained by the chosen sampling method of OHS, as the thrust values were affected by all of the casing geometry inputs, thus generating a warped scatter distribution. However, it can be inferred that large inlet lip radius generally tends to generate greater thrust. As stated previously, this is due to the large inlet lips maximizing the duct intake area affected by the low-pressure region just ahead of the rotating fan blades. This will not only cause the air mass flow to increase, but also generate more duct thrust. The same may also be true for how the inlet lip affects the fan's efficiency, as the faster airflow entering the ducted fan will undoubtedly reduce the fan blades' induced drag, therefore reducing the required power. It may also be possible to deepen the research by raising the inlet lip radius' maximum limit from the limits shown in Table 3, thus further exploring the parameter's influence on the EDF's performance.

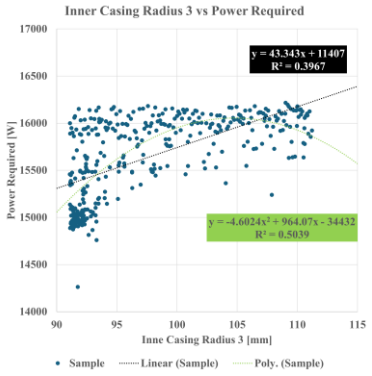

Figure 11 Scatter plot for power required against Inner Casing Radius 3

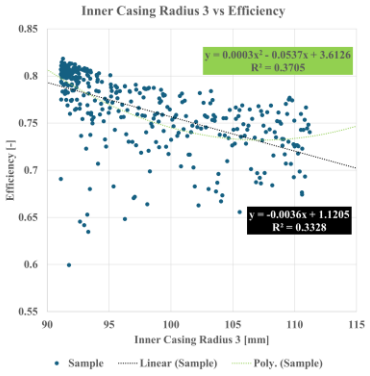

Figure 12 Scatter plot for efficiency against Inner Casing Radius 3

Similar to previous analysis on the influence of inlet lip radius on the ducted fan's performance, the widespread distribution of the scatter plot may cause misinterpretation. However, it can be inferred that generally, increasing the Inner Casing Radius 3 will raise the power required and reduce the ducted fan's efficiency. This is because increasing the diameter of the inner casing just ahead of the fan blades may damage the airflow just before flowing past the fan blades, thus generating turbulence, and reducing the fan blade's efficiency.

4 Conclusion

A linear and nonlinear correlation analysis between a 195 mm ducted fan geometry, consisting of a single rotating fan blade with a row of stator blades behind it, and its performance has been carried out. Based on the findings previously discussed, it is found that the EDF's inlet lip diameter shows the largest influence on its total thrust, as a large inlet lip diameter will not only raise the mass air flow entering the fan, but also maximize the surface area of the duct casing which is affected by the low-pressure region ahead of the fan. Lastly, the diameter of the casing's inner section and the exhaust length displays significant influence on the ducted fan's propulsive efficiency.

Finally, future research can be explored on other forms of EDF, such as contra-rotating ducted fans with multiple rotating fan blades, as well as on how the ducted fan's design affects its performance in varying external conditions, such as during cruising phase, etc. Additionally, there is a potential for further studies regarding optimization methods to help achieve the most optimum ducted fan designs.

5 Acknowledgement

This research was not funded by any grant.

6 Nomenclature

List the nomenclature in alphabetical order. List Roman letters followed by Greek symbols followed by subscript and superscripts.

p	=	Static pressure
S_f	=	Cross-section area of the fan's stream tube
P_{gen}	=	Generated power by the EDF
P_{req}	=	Required power to turn the fan
S_f	=	Cross-section area of the fan's stream tube
T	=	Thrust
η	=	Efficiency
Ω	=	Fan rotation speed
θ_{xyz}	=	Angle against EDF's axis
τ	=	Torque
τ_w	=	Viscous force

7 References

[1] Hu, J., Niu, H., Carrasco, J., Lennox, B. & Arvin, F., *Fault-Tolerant Cooperative Navigation of Networked UAV Swarms for Forest Fire Monitoring*, Aerospace Science and Technology, **123**, pp. 1-12, 2022.

[2] Ai, T., Xu, B., Xiang, C., Fan, W., & Zhang, Y., *Modeling of a Novel Coaxial Ducted Fan Aerial Robot Combined with Corner Environment by Using Artificial Neural Network*, Sensors, **20**, pp. 1-25, 2020.

[3] Choi, H., Sturdza, P., & Murray, R. M., *Design and Construction of a Small Ducted Fan Engine for Nonlinear Control Experiments*, in American Control Conference, pp. 2618-262, 1994.

[4] Pereira, J. L., *Hover and Wind-Tunnel Testing of Shrouded Rotors for Improved Micro Air Vehicle Design*, PhD dissertation, University of Maryland, 2008.

[5] Wallis, R. A., *Axial Flow Fand Ducts*, John Wiley & Sons, 1983.

[6] Pfimlin, J. M., Binetti, P., Souères, P., Hamel, T., & Trouchet, D., *Modelling & Atittude Control Analysis of a Ducted Fan Micro*

Aerial Vehicle, Control Engineering Practice, **18**, pp. 209-218, 2009.
[7] Li, H. & Liu, K, *Aerodynamic Design Optimization and Analysis of Ducted Fan Blades in DEP UAVs*, Aerospace, **10**, pp. 1-13, 2023.
[8] Prisacariu, V., Ionica, C., & Boscoiuanu, M., *Flying Wing with Electric Ducted Fan (EDF) Propulsion*, in NCAS, 2013.
[9] Schaller, D. F., *A Technique for Shape Optimization of Ducted Fans*, PhD dissertation, Iowa State University, 2007.
[10] Ohanian, O. J., *Ducted Fan Aerodynamics and Modelling, with Applications of Steady and Synthetic & Jet Flow Control*, Virginia Polytechnic Institute and State University, 2011.
[11] Koç, S. T., Yılmaz, S., Erdem, D., & Kavsaoğlu, M. Ş., *Experimental Investigation of a Ducted Propeller*, in 4th European Conference for Aerospace Sciences (EUCASS), 2011
[12] Bontempo, R. & Manna, M., *Effects of Duct Casing Cross Section Camber and Thickness on the Performance of Ducted Propulsion Systems for Aeronautical Applications*, International Journal of Aerospace Engineering, 2016.
[13] le Roux, F. N., *The CFD Simulation of an Axial Flow Fan*. PhD dissertation, Stellebbosch University, 2010.
[14] Jung, Y. K., Jeon, K. S., Choi, C. K., Maxim, T., Kim, S., & Lee, J. W., *Configuration Design and Optimization of Ducted Fan Using Parameter-Based Design*, in 7th European Conference for Aeronautics and Space Sciences (EUCASS), 2015.
[15] Drela, M. & H. Youngren, *Axisymmetric Analysis and Design of Ducted Rotors*, 2005. https://web.mit.edu/drela/Public/web/dfdc/
[16] Abdurrahman, S., *Numerical Analysis on the Influence of Geometrical Variation on the Performance of a 195 mm Electric Ducted Fan*, Institut Teknologi Bandung, 2021.
[17] Gudmunsson, S., *General Aviation Aircraft Design: Applied Methods and Procedures*, 2nd ed., Butterworth-Heinemann, 2022.
[18] Menter, F. R., Kuntz, M., & Langtry, R., *Ten Years of Industrial Experience with the SST Turbulence Model*, in the 4th Internal Symposium on Turbulence, Heat and Mass Transfer, pp. 625-632, 2003.
[19] Menter, F. R., *Two-Equation Eddy-Viscosity Turbulence Models for Engineering Applications*, AIAA Journal, **32**, pp. 1598-1605, 1994.

[20] Queipo, N. V., Haftka, R. T., Shyy, W., Goel, T., Vaidyanathan, R., & Tucker, P. K., *Surrogate-Based Analysis and Optimization*, Progress in Aerospace Sciences, **41**, pp. 1-28, 2005.
[21] ANSYS DesignXplorer User's Guide, ANSYS Inc, 2022
[22] Pereira, A., & Broed, R., *Methods for Uncertainty and Sensitivity Analysis: Review and recommendations for implementation in Ecolego*, PhD dissertation, Stockholm Center of Physics, 2006.